floras, angiosperms typically constitute only a very small percentage of the total diversity[15,17,29]—perhaps reflecting low pollen production and poor dispersal abilities associated with insect pollination. Similarly, with one strongly disputed exception angiosperm wood has not been recorded from Aptian or older rocks, and angiosperm leaves in Aptian or earlier floras are also extremely rare. However, exceptionally preserved whole plants reported from the Lower Cretaceous Crato Formation, Brazil, document that diverse herbaceous water plants were present by the Aptian–Albian and were a prominent part of the angiosperm assemblage of this flora[21]. These observations suggest that the apparent discrepancy between the diversity of angiosperm reproductive structures and the diversity of leaves and wood during the earliest phases of angiosperm diversification may in part be explained by the low potential of leaves and stems of herbaceous plants, including water lilies and monocots, to be preserved.

Received 20 October; accepted 15 December 2000.

1. Qiu, Y.-L. *et al.* The earliest angiosperms: evidence from mitochondrial, plastid and nuclear genomes. *Nature* **402,** 404–407 (1999).
2. Qiu, Y.-L. *et al.* Phylogeny of basal angiosperms: analyses of five genes from three genomes. *Int. J. Plant Sci.* **161** (Suppl. 6), S3–S27 (2000).
3. Soltis, P. S., Soltis, D. E. & Chase, M. W. Angiosperm phylogeny inferred from multiple genes as a tool for comparative biology. *Nature* **402,** 402–404 (1999).
4. Kuzoff, R. A. & Gasser, C. S. Recent progress in reconstructing angiosperm phylogeny. *Trends Plant Sci.* **5,** 330–336 (2000).
5. Friis, E. M., Pedersen, K. R. & Crane, P. R. Angiosperm floral structures from the Early Cretaceous of Portugal. *Pl. Syst. Evol.* **8** (Suppl.), 31–49 (1994).
6. Magallón, S., Crane, P. R. & Herendeen, P. S. Phylogenetic pattern, diversity and diversification of eudicots. *Ann. Missouri Bot. Gard.* **86,** 297–372 (1999).
7. Frumin, S. & Friis, E. M. Magnoliid reproductive organs from the Cenomanian–Turonian of northwestern Kazakhstan: Magnoliaceae and Illiciaceae. *Plant Syst. Evol.* **216,** 265–288 (1999).
8. Gandolfo, M. A., Nixon, K. C. & Crepet, W. L. in *Monocots: Systematics and Evolution* (eds Wilson, K. I. & Morrison, D. A.) 44–51 (CSIRO, Melbourne, 2000).
9. Friis, E. M., Pedersen, K. R. & Crane, P. R. Early angiosperm diversification: the diversity of pollen associated with angiosperm reproductive structures in Early Cretaceous floras from Portugal. *Ann. Missouri Bot. Gard.* **86,** 259–296 (1999).
10. Friis, E. M., Pedersen, K. R. & Crane, P. R. Reproductive structure and organization of basal angiosperms from the Early Cretaceous (Barremian or Aptian) of Western Portugal. *Int. J. Plant Sci.* **161** (Suppl. 6), S169–S182 (2000).
11. Zbyszewski, G., Manupella, G. & Da Veiga Ferreira, O. *Carta geológica de Portugal na escala de 1/50 000. Notícia explicativa da folha 27-A Vila Nova de Ourém* (Serviços Geológicos de Portugal, Lisbon, 1974).
12. Doyle, J. A. & Hickey, L. J. in *Origin and Early Evolution of Angiosperms* (ed. Beck, C. B.) 139–206 (Columbia Univ. Press, New York, 1976).
13. Penny, J. H. J. An Early Cretaceous angiosperm pollen assemblage from Egypt. *Special Papers Palaeontol.* **35,** 121–134 (1986).
14. Doyle, J. A. Revised palynological correlations of the lower Potomac Group (USA) and the Cocobeach sequence of Gabon (Barremian–Aptian). *Cretaceous Res.* **13,** 337–349 (1992).
15. Hughes, N. F. & McDougall, A. B. Barremian-Aptian angiospermid pollen records from southern England. *Rev. Palaeobot. Palynol.* **65,** 145–151 (1990).
16. Doyle, J. A. & Robbins, E. I. Angiosperm pollen zonation of the continental Cretaceous of the Atlantic Coastal Plain and its application to deep wells in the Salisbury Embayment. *Palynology* **1,** 43–78 (1977).
17. Hughes, N. F. *The Enigma of Angiosperm Origins* (Cambridge Univ. Press, Cambridge, 1994).
18. Rey, J. Recherches géologiques sur le Crétacé inférieur de l'Estremadura (Portugal). *Serviços Geológicos de Portugal, Memórias (Nova Série) 3* **21,** 1–477 (1972).
19. Endress, P. K. & Igersheim, A. Gynoecium structure and evolution in basal angiosperms. *Int. J. Plant Sci.* **161** (Suppl. 6), S211–S223 (2000).
20. Saporta, G. D. *Flore fossile du Portugal. Nouvelles contributions à la flore Mésozoique. Accompagnées d'une notice stratigraphique par Paul Choffat* (Imprimerie de l'Academie Royale des Sciences, Lisbon, 1894).
21. Mohr, B. & Friis, E. M. Early angiosperms from the Aptian Crato Formation (Brazil), a preliminary report. *Int. J. Plant Sci.* **161** (Suppl. 6), S155–S167 (2000).
22. Les, D. H. *et al.* Phylogeny, classification and floral evolution of water lilies (Nymphaeaceae; Nymphaeales): A synthesis of non-molecular, *rbcL*, *matK*, and rDNA data. *Syst. Bot.* **24,** 28–46 (1999).
23. Williamson, P. S. & Schneider, E. I. Cabombaceae. in *The Families and Genera of Vascular Plants. II Flowering plants—Dicotyledons. Magnoliid, Hamamelid and Caryophyllid Families* (eds Kubitzki, K., Rohwer, J. G. & Bittrich, V.) 157–161 (Springer, Berlin, 1993).
24. Schneider, E. l. & Williamson, P. S. Nymphaeaceae. in *The Families and Genera of Vascular Plants. II Flowering plants—Dicotyledons. Magnoliid, Hamamelid and Caryophyllid Families* (eds. Kubitzki, K., Rohwer, J. G. & Bittrich, V.) 486–493 (Springer, Berlin, 1993).
25. Bessey, C. E. The phylogenetic taxonomy of flowering plants. *Ann. Missouri Bot. Gard.* **2,** 109–164 (1915).
26. Takhtajan, A. *Flowering Plants. Origin and Dispersal* (Oliver & Boyd, Edinburgh, 1969).
27. Drinnan, A. N., Crane, P. R. & Hoot, S. B. Patterns of floral evolution in the early diversification of non-magnoliid dicotyledons (eudicots). *Plant Syst. Evol.* **8** (Suppl.), 93–122 (1994).
28. Friis, E. M., Crane, P. R. & Pedersen, K. R. in *Evolution and Diversification of Land Plants* (eds Iwatsuki, K. & Raven, P. H.) 121–156 (Springer, Tokyo, 1997).
29. Brenner, G. J. & Bickoff, I. S. Palynology and the age of the Lower Cretaceous basal Kurnub Group from the coastal plain to the northern Negev of Israel. *Palynology* **16,** 137–185 (1992).

Acknowledgements

We thank P. K. Endress and J. Schönenberger for valuable comments and help; and P. von Knorring for preparing the reconstruction of the fossil flower. The work was supported by grants from the Swedish Natural Science Foundation (to E.M.F.), the Carlsberg Foundation (to K.R.P. and E.M.F.), the Danish Natural Science Research Council (to K.R.P.) and the US National Science Foundation (to P.R.C.).

Correspondence and requests for materials should be addressed to E.M. Friis (e-mail: else.marie.friis@nrm.se).

Mesoscale vertical motion and the size structure of phytoplankton in the ocean

Jaime Rodríguez*, Joaquín Tintoré†, John T. Allen‡, José Mª Blanco*, Damià Gomis†, Andreas Reul*, Javier Ruiz§, Valeriano Rodríguez*, Fidel Echevarría§ & Francisco Jiménez-Gómez*‖

** Departamento de Ecología, Universidad de Málaga, Campus de Teatinos, 29071-Málaga, Spain*
† Institut Mediterrani d'Estudis Avançats (CSIC-UIB), 07071 Palma de Mallorca, Spain
‡ Southampton Oceanography Center, J. Rennell Division, Southampton SO14 3ZH, UK
§ Departamento de Biología Animal, Biología Vegetal y Ecología, Facultad de Ciencias del Mar, Universidad de Cádiz, 11510 Puerto Real, Cádiz, Spain

Phytoplankton size structure is acknowledged as a fundamental property determining energy flow through 'microbial' or 'herbivore' pathways[1]. The balance between these two pathways determines the ability of the ecosystem to recycle carbon within the upper layer or to export it to the ocean interior[1]. Small cells are usually characteristic of oligotrophic, stratified ocean waters, in which regenerated ammonium is the only available form of inorganic nitrogen and recycling dominates. Large cells seem to characterize phytoplankton in which inputs of nitrate enter the euphotic layer and exported production is higher[2–4]. But the size structure of phytoplankton may depend more directly on hydrodynamical forces than on the source of available nitrogen[5–7]. Here we present an empirical model that relates the magnitude of mesoscale vertical motion to the slope of the size–abundance spectrum[8–10] of phytoplankton in a frontal ecosystem. Our model indicates that the relative proportion of large cells increases with the magnitude of the upward velocity. This suggests that mesoscale vertical motion—a ubiquitous feature of eddies and unstable fronts—controls directly the size structure of phytoplankton in the ocean.

The oceanic mesoscale, 10–100 km, is the equivalent of the atmospheric storm scale. It is generally considered to be the most energetic scale, and it is where fronts between water masses become unstable and strong three-dimensional circulations are set up. Fronts are places of enhanced biological activity and, from the biological point of view, vertical circulation is of great significance to primary productivity as it may explain the patchiness of primary productivity in the surface layers of the ocean and the patchiness of nutrient distributions[11]. During the OMEGA (Observations and

‖ Present address: Departamento de Biología Animal, Biología Vegetal y Ecología, Facultad de Ciencias Experimentales, Universidad de Jaén, 23071 Jaén, Spain.

Modelling of Eddy Scale Geostrophic and Ageostrophic Circulation) project, multidisciplinary observations were made in the northwestern Alborán (Mediterranean) Sea, where water of Atlantic and Mediterranean origin meet, creating gyres, fronts and eddies of different scales. This sea is an ideal region in which to study physical–biological coupling, particularly the relation between vertical motion and the size structure of phytoplankton.

If vertical motion controls the size structure of phytoplankton, the slope of the community size–abundance spectrum (SAS; see Methods) should be less negative in areas of upward motion than in areas of downward motion, because upward motion increases the residence time of large cells in the upper layer against their tendency to sink. Small cells, on the other hand, do not sink (or sink very slowly) because of the dominance of viscosity at very low Reynolds numbers; therefore, vertical motion would not have a differential effect on this part of the community SAS. Ideally there should be a positive correlation between the magnitude of the upward vertical velocity (w) and the flatness of the spectrum linear model, owing to the increased retention of large cells within the upper layers. The relation obtained for our complete set of observations was not so simple (Fig. 1a); however, a linear relationship between vertical velocity and size spectrum slope was clearly evident for vertical velocity magnitudes of less than 5–6 m d^{-1} (Fig. 1b):

$$\text{SAS slope} = -0.944 + 0.033w \ (\text{in m d}^{-1}) \qquad (1)$$

($r^2 = 0.683$, $\alpha < 0.001$; 95% confidence interval (CI) for the regression slope: 0.025–0.042). Our conceptual model indicates that there may be a positive relation between the magnitude of the mesoscale vertical motion and the slope of the SAS of phytoplankton. If the size structure of phytoplankton were nutrient dependent, we would expect a different relation between vertical velocity and SAS slope at the depth of the 'deep chlorophyll maximum' (DCM), where cells are expected to find optimal growth conditions in the vicinity of the nutricline.

This is not the case (Fig. 1b), and the relation is the same for assemblages at, over, or below the DCM. This suggests that nutrients are not the critical factor controlling the size structure of the community. We would expect, however, a light-related effect on the DCM size structure, as when the DCM occurs very deep in the water column it seems to be characterized by small cells and low amounts of chlorophyll, whereas the opposite occurs in the case of a shallow DCM[4,12,13]. Our observations do not support this hypothesis (Fig. 2). In fact, the size spectrum with the least negative slope corresponds to a very deep DCM community (Fig. 3), whereas spectra very similar in shape (Fig. 2) correspond to DCM layers placed at very different depths within the water column (Fig. 3). In all the cases, size distributions are highly similar up to cell sizes around 5 μm equivalent spherical diameter and diverge for larger cells with higher sinking velocities. This divergence illustrates the size-dependent, counteracting effect of upward vertical motion and implies that, on relative terms, the flatter spectrum has around seven times the biomass of steeper spectra in the size range of cells between 10^4 μm^3 (~25 μm diameter) and 10^5 μm^3 (~60 μm diameter).

Hypotheses about the vertical motion control on the size of planktonic organisms were previously proposed at two very different scales. At the scale of tens of metres, which characterizes Langmuir circulation, the coupled upwelling and downwelling processes were considered to be responsible for the accumulation

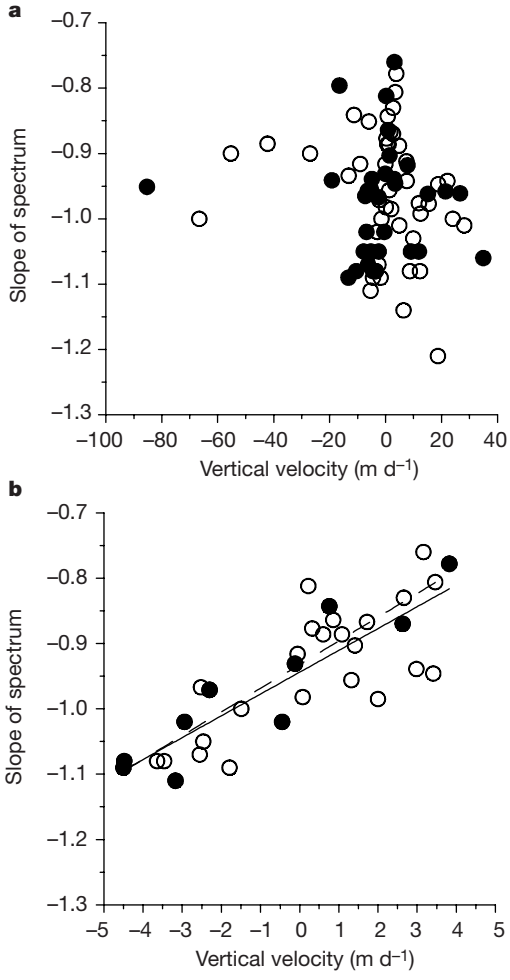

Figure 1 Slope of the size–abundance spectrum plotted against the magnitude of vertical velocity (w) diagnosed for mesoscale instability. **a**, For the full range of w, filled circles represent observations below the thermocline that can be considered free from the influence of mixed layer mixing processes. **b**, Data points and a linear regression (continuous line) for w in the range between ± 5 m d^{-1}; filled circles represent measurements at the depth of DCM, described by the model (broken line): SAS slope = –0.932 + 0.036w ($r^2 = 0.854$; $\alpha < 0.001$; 95% CI for the regression slope = 0.024–0.048).

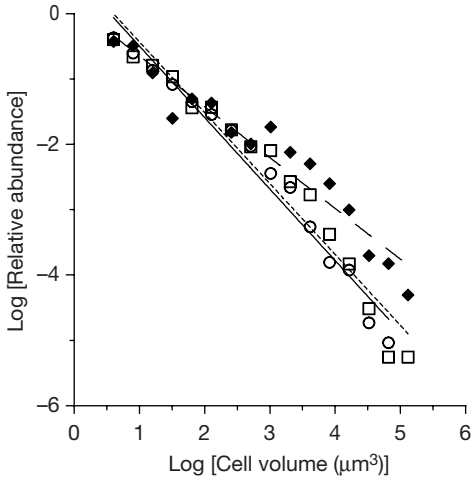

Figure 2 Size–abundance spectra of DCM phytoplankton communities at the spots of highest upward and downward vertical velocity in the range considered in Fig. 1b. Filled diamonds, DCM community placed at 60 m depth, w = +3.8 m d^{-1}; open squares, 30 m depth, w = –4.8 m d^{-1}; open circles, 50 m depth, w = –4.8 m d^{-1}. Abundance is expressed in relative units to eliminate differences in absolute biomass between spectra. For filled diamonds, $r^2 = 0.934$ ($\alpha < 0.001$); regression slope = –0.778 (95% CI = –0.897, –0.660); for open squares, $r^2 = 0.952$ ($\alpha < 0.001$); regression slope = –1.085 (95% CI = –1.224, –0.946); for open circles, $r^2 = 0.972$ ($\alpha < 0.001$); regression slope = –1.095 (95% CI = –1.207, –0.983).

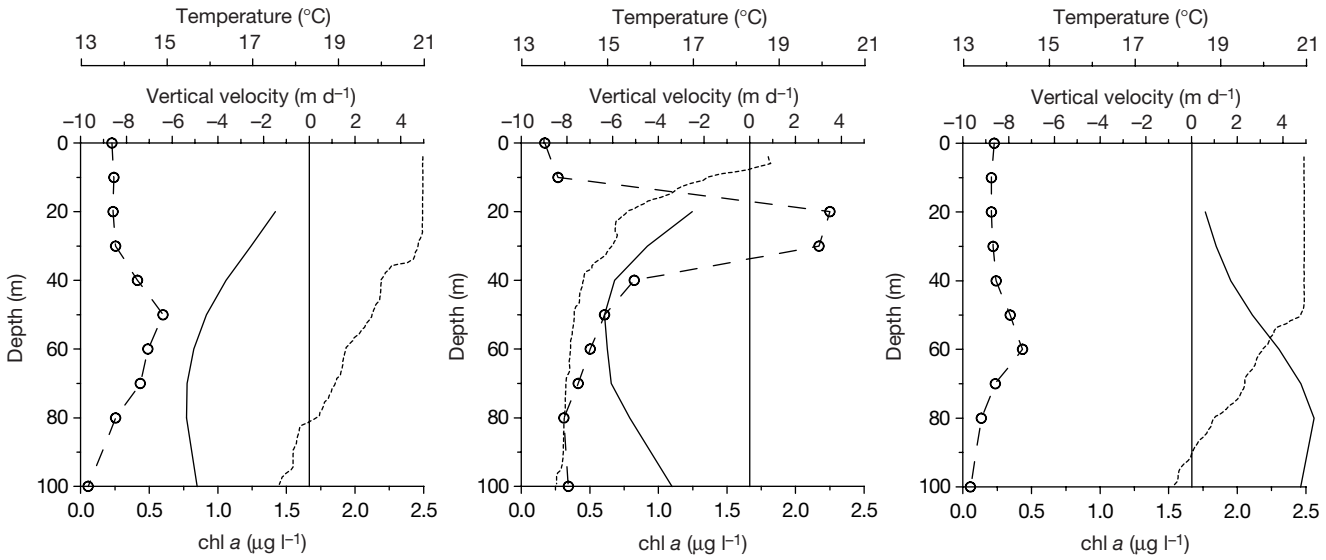

Figure 3 Vertical structure of the water column corresponding to size–abundance spectra in Fig. 2. Continuous line, vertical velocity; dotted line, temperature; open circles, chlorophyll (chl) concentration.

of organisms with negative or positive buoyancy (a size-related property)[14]. At the biogeographical, large scale of oceanic regions in the Pacific Ocean, it has been proposed that average cell diameter is the largest in regions of weak ascending and weak descending motion, and that it is the smallest in areas of most intensive vertical motion[5,6]. Notably, a linear relation between cell diameter and vertical motion for the range of weak velocities at the large scale of oceanic convergences and divergences has been reported[5].

Observations about the size distribution of fractionated chlorophyll in the equatorial Pacific are also better interpreted in terms of circulation (equatorial upwelling and horizontal transport) rather than a nutrient effect[7]. There have been no previous published studies relating the vertical component of mesoscale fluid flow to the size structure of the primary producer community for two main reasons. First, mesoscale vertical velocities are too small to be measured directly using traditional vessel mounted or moored acoustic current profilers and therefore they have to be determined (see Methods) through careful analysis of high-resolution hydrographic measurements and assumed balance conditions for the flow[15–17]. Second, determining the SAS of the planktonic community (see Methods) is a time-consuming task frequently substituted by average descriptors such as "net-plankton, cell average diameter"[5,6] or bulk variables such as "size-fractionated chlorophyll"[7].

The impossibility of discriminating a nutrient-mediated effect of mesoscale vertical motion on the size structure of phytoplankton at the DCM layer gives support to the existence of a direct vertical motion control on community structure, and suggests that the interaction between water vertical motion and cell sinking properties are the primary forces in shaping the size-abundance spectrum of phytoplankton in the upper layer of the ocean. Biological processes such as photo-adaptation, nutrient uptake and growth, and cell motility would determine other DCM properties like species composition or chlorophyll and biomass concentration, usually analysed to explain the origin and maintenance of the DCM layer and the vertical distribution of phytoplankton in general[18–21].

However, we have to question why the interaction between vertical motion and size structure is limited to weak magnitude of vertical velocity. There are several, non-mutually exclusive explanations to be considered. The first is principally a sampling problem. Generally, the magnitude of vertical velocity is inversely related to the scale of the horizontal flow field[16,22,23]. For example, vertical velocities estimated from the curl of the wind stress[5,6] are typically in the range of $\pm 10^{-1}$ m d^{-1}. In highly energetic mesoscale flows like ours, vertical velocities between 10 and 100 m d^{-1} (refs 16, 17, 24) are more typical, but are associated with strong advection (in our case up to 1.5 m s^{-1}) that make it difficult to make synoptic observations and result in vertical motion estimates that are susceptible to large errors[25]. Consequently, it is out of the centre of the frontal jet, where the observations are more truly synoptic that we can have most confidence in our results and where the magnitude of the vertical velocity is lowest.

Second, mesoscale, ageostrophic vertical motion can be modified by other physical processes like wind-driven turbulence in the uppermost layer, tidal oscillations or internal waves at the thermocline that might contribute to the scatter of points at high vertical velocities. To avoid contamination with mixed layer processes, we have identified those data points below the thermocline (Fig. 1a). Both the complete data set and the subset containing data only from below the thermocline show similar scatters against vertical velocity magnitude, however, indicating that wind-driven turbulence is not the origin of the scatter. It is more difficult to avoid contamination from internal waves, but the SeaSoar hydrographic sections show no evidence of significant internal wave activity in the region.

All this suggests that the interaction of mesoscale vertical motion with other physical processes is probably of less importance in explaining the scatter of points at high values of vertical velocity. In the third place, the interaction between upward water motion and the sinking velocity of cells should be considered. The calculated range of vertical velocities includes the sinking velocities of phytoplanktonic cells even for the largest sizes[14]. The largest cells included in our size–abundance spectrum (Fig. 2) have diameters between 60 and 70 μm and, according to Smayda's model[14], they would sink at 2–2.5 m d^{-1}. Thus, the range of vertical velocities in Fig. 1b is of the same order as the range of the size-dependent sinking velocity of the cells included in our SAS analysis. This suggests that only a relatively small upward water motion is needed to support phytoplanktonic cells in the size range analysed, which certainly contains the bulk of ocean primary producers. Consequently, an extended mathematical model for the whole range of vertical velocity values shown in Fig. 1 would need a much broader SAS analysis including large particles such as colonies, aggregrates and fecal pellets. Such an analysis would permit the complete evaluation of the role of mesoscale dynamics in controlling the size structure of pelagic particles and its impact on the vertical flux of carbon in the ocean. □

Methods

Modelling the SAS of phytoplankton

We counted and measured phytoplanktonic cells by using a video-interactive, microscopy-image analysis system that permits the discrimination and elimination of detritus and other non-living particles. Individual linear measurements were transformed into estimations of cell volume through numerical computation, and these were then distributed along an octave ($\log_2$) scale of cell volume. Finally, a regression mode 1 was applied to the log-transformed values of cell abundance (y axis, cells per ml) and cell volume (x axis, μm^3). The resulting key parameter is the slope (b) of the regression model:

$$\log[\text{cell abundance (cells per ml)}] = a - b\log[\text{cell volume } (\mu m^3)]$$

A general account of methods for the analysis of the size structure of planktonic communities can be found in ref. 10.

Computation of vertical velocity

In the framework of the Quasi-Geostrophic (QG) approximation, the vertical component of the velocity field (w) can be estimated from a diagnostic equation known as the Omega equation[26]. This equation can be solved in a three-dimensional domain provided that (1) the QG vertical forcing is know at every point of the domain; and (2) boundary conditions are specified. The vertical forcing term can be computed by finite differences from hydrographic data alone (for example, from density and/or dynamic height data), which must have been previously interpolated from stations to a regular grid. Regarding boundary conditions, we assumed $w = 0$ at the bottom and surface, and Neumann conditions at the lateral boundaries[27]. Several tests show that the sensitivity of vertical velocity fields to lateral boundaries restricts to the few outermost grid points, with no significant influence on the results obtained in the inner domain.

Received 6 September 2000; accepted 3 January 2001.

1. Legendre, L. & Le Fèvre, J. in *Productivity of the Ocean: Present and Past* (eds Berger, W. H., Smetaceck, V. S. & Wefer, G.) 49–63 (John Wiley & Sons Limited, New York, 1989).
2. Eppley, R. W. & Peterson, B. J. Particulate organic matter flux and planktonic new production in the deep ocean. *Nature* **282,** 677–680 (1979).
3. Malone, T. C. in *The Physiological Ecology of Phytoplankton* (ed. Morris, I.) 433–464 (Blackwell Scientific Publications, Oxford, 1980).
4. Chisholm, S. W. in *Primary Productivity and Biogeochemical Cycles in the Sea* (eds Falkowski, P. G. & Woodhead, A. D.) 213–237 (Plenum, New York, 1992).
5. Semina, H. J. Water movement and the size of phytoplankton cells. *Sarsia* **34,** 267–272 (1968).
6. Semina, H. J. The size of phytoplankton cells in the Pacific Ocean. *Int. Revue ges. Hidrobiol.* **57,** 177–205 (1972).
7. Peña, A., Lewis, M. R. & Harrison, G. Primary productivity and size structure of phytoplankton biomass on a transect of the equator at 135°W in the Pacific Ocean. *Deep-Sea Res.* **37,** 295–315 (1990).
8. Platt, T. & Denman, K. H. The structure of pelagic marine ecosystems. *Rapp. P.-V. Reun. Cons. Int. Explor. Mer* **173,** 60–65 (1978).
9. Rodríguez, J. & Mullin, M. M. Relation between biomass and body weight of plankton in a steady state oceanic ecosystem. *Limnol. Oceanogr.* **31,** 361–370 (1986).
10. Rodríguez, J. & Li, W. K. W. (eds) The size structure and metabolism of the pelagic ecosystem. *Scientia Marina* **58,** 1–167 (1994).
11. Strass, V. H. Chlorophyll patchiness caused by mesoscale upwelling at fronts. *Deep-Sea Res.* **39,** 75–96 (1992).
12. Harris, G. P., Ganf, G. G. & Thomas, D. P. Productivity, growth rates and cell size distributions of phytoplankton in the SW Tasman Sea: implications for carbon metabolism in the photic zone. *J. Plankton Res.* **9,** 1003–1030 (1987).
13. Rodríguez, J. *et al.* Patterns in the size structure of phytoplankton community in the deep fluorescence maximum of the Alboran Sea (southwestern Mediterranean). *Deep-Sea Res.* **45,** 1577–1593 (1998).
14. Smayda, T. J. The suspension and sinking of phytoplankton in the sea. *Oceanogr. Mar. Biol. Annu. Rev.* **8,** 353–414 (1970).
15. Leach, H. The diagnosis of synoptic-scale vertical motion in the seasonal thermocline. *Deep-Sea Res.* **34,** 2005–2017 (1987).
16. Tintoré, J., Gomis, D., Alonso, S. & Parrilla, G. Mesoscale dynamics and vertical motion in the Alboran Sea. *J. Phys. Oceanogr.* **21,** 811–823 (1991).
17. Allen, J. T. & Smeed, D. A. Potential vorticity and vertical velocity at the Iceland Faroes front. *J. Phys. Oceanogr.* **26,** 2611–2634 (1996).
18. Cullen, J. J. The deep chlorophyll maximum: comparing vertical profiles of chlorophyll a. *Can. J. Fish. Aquat. Sci.* **39,** 791–803 (1982).
19. Furuya, K. & Marumo, R. The structure of the phytoplankton community in the subsurface chlorophyll maxima in the western North Pacific Ocean. *J. Plankton Res.* **5,** 393–406 (1983).
20. Estrada, M. *et al.* Variability of deep chlorophyll maximum characteristics in the Northwestern Mediterranean. *Mar. Ecol. Prog. Ser.* **92,** 289–300 (1993).
21. Ruiz, J., García, C. M. & Rodríguez, J. Vertical patterns of phytoplankton size distribution in the Cantabric and Balearic seas. *J. Mar. Systems* **9,** 269–282 (1996).
22. Fiekas, V., Leach, H., Mirbach, K.-J. & Woods, J. D. Mesoscale inestability and upwelling. Part 1: Observations at the North Atlantic intergyre front. *J. Phys. Oceanogr.* **24,** 1750–1758 (1994).
23. Viúdez, A., Tintoré, J. & Haney, R. L. Circulation in the Alboran Sea as determined by quasi-synoptic hydrographic observations. I. Three dimensional structure of the two anticyclonic gyres. *J. Phys. Oceanogr.* **26,** 684–705 (1996).
24. Pollard, R. T. & Regier, L. Large variations in potential vorticity at small spatial scales in the upper ocean. *Nature* **348,** 227–229 (1990).
25. Allen, J. T., Smeed, D. A., Nurser, A. J. G., Zhang, J. W. & Rixen, M. Diagnosing vertical velocities with the QG omega equation: an examination of the errors due to sampling strategy. *Deep-Sea Res.* (in the press).
26. Cushman-Roisin, B. *Introduction to Geophysical Fluid Dynamics* (Prentice-Hall, Englewood Cliffs, New Jersey, 1994).
27. Gomis, D., Ruíz, S. & Pedder, M. A. Diagnostic analysis of the 3D ageostrophic circulation from a Multivariate Spatial Interpolation of CTD and ADCP data. *Deep-Sea Res.* **48,** 269–295 (2000).

Acknowledgements

This work was supported by the MAST III programme of the European Commision and the CICYT-CYTMAR programme (Spain). We thank M. Emelianov for translating the Russian work of H. J. Semina. We also thank the officers, technicians and crew of *BIO Hesperides* for their help during the OMEGA cruise.

Correspondence and requests for materials should be addressed to J.R. (e-mail: jaime@uma.es).

Ecological importance of trichromatic vision to primates

Nathaniel J. Dominy & Peter W. Lucas

Department of Anatomy, University of Hong Kong, 5 Sassoon Road, Hong Kong, People's Republic of China

Trichromatic colour vision, characterized by three retinal photopigments tuned to peak wavelengths of ~430 nm, ~535 nm and ~562 nm (refs 1, 2), has evolved convergently in catarrhine primates and one genus of New World monkey, the howlers (genus *Alouatta*)[3]. This uniform capacity to discriminate red–green colours, which is not found in other mammals, has been proposed as advantageous for the long-range detection of either ripe fruits[4,5] or young leaves[6] (which frequently flush red in the tropics[7]) against a background of mature foliage[8,9]. Here we show that four trichromatic primate species in Kibale Forest, Uganda, eat leaves that are colour discriminated only by red–greenness, a colour axis correlated with high protein levels and low toughness. Despite their divergent digestive systems, these primates have no significant interspecific differences in leaf colour selection. In contrast, eaten fruits were generally discriminated from mature leaves on both red–green and yellow–blue channels and also by their luminance, with a significant difference between chimpanzees and monkeys in fruit colour choice. Our results implicate leaf consumption, a critical food resource when fruit is scarce[10], as having unique value in maintaining trichromacy in catarrhines.

In Kibale National Park, Uganda, leaves eaten by trichromatic chimpanzees (*Pan troglodytes*), black-and-white colobus (*Colobus guereza*), red colobus (*Piliocolobus badius*) and red-tailed monkeys (*Cercopithecus ascanius*) could be discriminated from mature leaves in colour only by the red–green channel (Fig. 1a). Consumed leaves, which included some leaves of mature status, had a higher average luminance, but the red–green colour channel was a far better discriminant (Fig. 1b), primarily because many young red leaves were dark. There were no significant differences overall between primate species in the colours of leaves eaten (Duncan's multiple range test, $P > 0.05$), and the red–greenness of the leaves was highly positively correlated with the ratio of protein content to toughness (Spearman's test, $R = 0.58$, $P < 0.001$). This ratio was consistently higher in leaves consumed by each primate than in mature foliage (Fig. 2).

In contrast, eaten fruits were distinguishable on both the red–green and yellow–blue colour channels (Fig. 3), as well as luminance (Duncan's multiple range test, $P < 0.001$ for each case). Fruits selected by monkeys were more yellow than mature foliage ($P < 0.03$), whereas those eaten by chimpanzees were significantly more yellow than those eaten by monkeys (Duncan's multiple range